U.S. DEPARTMENT OF ENERGY | Office of Science

DOE/SC-ARM-19-028

Cloud, Aerosol, and Complex Terrain Interactions (CACTI) Field Campaign Report

A Varble
P Salio
P Borque
G McFarquhar
E Zipser
R Houze, Jr.
P Kollias
R Leung
D Romps
S Nesbitt
E Avila
P DeMott
S van den Heever
D Gochis
M Jensen
S Kreidenweis
K Rasmussen
C Williams

November 2019

ARM

DISCLAIMER

DOE/SC-ARM-19-028

Cloud, Aerosol, and Complex Terrain Interactions (CACTI) Field Campaign Report

A Varble, Pacific Northwest National Laboratory, University of Utah
Principal Investigator

Steve Nesbitt, University of Illinois
P Salio, Universidad de Buenos Aires
E Avila, Universidad Nacional de Córdoba
P Borque, University of Illinois
G McFarquhar, University of Oklahoma
S van den Heever, Colorado State University
E Zipser, University of Utah
D Gochis, National Center for Atmospheric Research
R Houze, Jr., University of Washington
M Jensen, Brookhaven National Laboratory
P Kollias, Stony Brook University
S Kreidenweis, Colorado State University
R Leung, Pacific Northwest National Laboratory
K Rasmussen, Colorado State University
D Romps, Lawrence Berkeley National Laboratory
C Williams, University of Colorado–Boulder
Co-Investigators

November 2019

Work supported by the U.S. Department of Energy,
Office of Science, Office of Biological and Environmental Research

Acronyms and Abbreviations

AAF	ARM Aerial Facility
AIMMS	Aircraft Integrated Meteorological Measurement System,
AMF	ARM Mobile Facility
AOD	aerosol optical depth
ARM	Atmospheric Radiation Measurement
AWS	automated weather station
CACTI	Cloud, Aerosol, and Complex Terrain Interactions
CCN	cloud condensation nuclei
CN	condensation nuclei
COW	C-band on Wheels
C-SAPR	C-band Scanning ARM Precipitation Radar
CSU	Colorado State University
CSWR	Center for Severe Weather Research
DOE	U.S. Department of Energy
DOW	Doppler on Wheels
EOL	Earth Observing Laboratory
EOP	extended operational period
FOV	field of view
G-1	Gulfstream-1
GPS	Global Positioning System
HSRHI	hemispheric range-height indicator
IOP	intensive operational period
IWGADTS	Interagency Working Group for Airborne Data and Telemetry Systems
Ka-SACR	Ka-band Scanning ARM Cloud Radar
KAZR	Ka-band ARM Zenith Radar
NCAR	National Center for Atmospheric Research
NOAA	National Oceanic and Atmospheric Administration
NSF	National Science Foundation
PI	principal investigator
PPI	plan position indicator
RAL	Research Applications Laboratory
RELAMPAGO	Remote sensing of Electrification, Lightning, And Mesoscale/microscale Processes with Adaptive Ground Observations
RH	relative humidity
RHI	range-height indicator

SMN	Servicio Meteorológico Nacional
SMPS	scanning mobility particle sizer
UIUC	University of Illinois at Urbana-Champaign
UPS	uninterruptable power supply
UTC	coordinated universal time
VAP	value-added product
WRF	Weather Research and Forecasting
X-SACR	X-band Scanning ARM Cloud Radar

Contents

Acronyms and Abbreviations iii
1.0 Summary 1
2.0 Results 15
3.0 Publications and References 17
  3.1 Journal Articles 18
  3.2 Presentations 18
  3.3 References 19

Figures

1 A map of the CACTI observing domain highlighting the Sierras de Córdoba mountain range, the AMF1 central site, nearby photogrammetric cameras (ACDC), upper-elevation meteorological stations, and the second sounding site at Villa Dolores. 5
2 A view west across the AMF1 site toward the crest of the Sierras de Córdoba mountain range (top). Aerial views of the AMF1 site with surrounding land cover looking toward the east-southeast (bottom left) and zoomed in on the site with directions shown (bottom right). 6
3 An idealized view of the CACTI measurement strategy showing typical flows and orographic cloud locations. 7
4 A map overlaid with the flight tracks from all 22 flights (left) showing the location of the airport in Rio Cuarto and the AMF1 site. The upper right picture is from an outreach event and the lower right picture shows cumulus congestus from Flight 10 with ice forming in one of the turrets. 8
5 The CACTI extended operational period and IOP within the context of the RELAMPAGO-Hydro and IOP timelines. 10
6 (a) KAZR reflectivity over a 1-hour period with (b) Ka-SACR reflectivity in a west-east HSRHI cross-section at one time during the hour. Mean Doppler velocity from the two radars are shown in (c) and (d), respectively. 13
7 A 7-day period in November 2018 showing AMF1 site (a) Pluvio-2 rain rate and accumulated rainfall, (b) 0.4% supersaturation CCN, (c) CN > 10 nm diameter concentration, and (d) aerosol size distribution from the SMPS. 14
8 Example HSRHIs from the X-SACR during a deep convective initiation and growth event showing (a-b) west-east cross-sections of reflectivity and mean Doppler velocity and (c-d) south-north cross-sections of the same variable where 0 is the location of the radar at the AMF1 site. 15

Tables

1 Ground instrumentation deployed for CACTI, the primary measurements or retrievals provided by instrumentation, and known periods with data quality issues. 2

2 CACTI G-1 flights including their date, time period, and primary target. 7

3 G-1 aircraft instrumentation during CACTI with primary measurements of each instrument and known data quality issues. 9

4 RELAMPAGO IOP time periods, mission type, and mobile instrumentation involved including the DOWs, Pods, and disdrometers from CSWR, and radiosondes from CSWR, UIUC, and CSU. ... 11

5 DOE ARM value-added products planned for CACTI including their current/planned availability. 15

6 CACTI days subjectively determined to have rainfall, deep convection, or cumulus/stratocumulus occur directly over the site using a combination of satellite, KAZR, and ceilometer data. 17

1.0 Summary

General circulation models and downscaled regional models exhibit persistent biases in deep convective initiation location and timing, cloud top height, stratiform area and precipitation fraction, and anvil coverage (e.g., Del Genio 2012, Del Genio et al. 2012, Hohenegger and Stevens 2013, Song et al. 2013). Despite important impacts on the distribution of atmospheric heating, moistening, momentum, and precipitation (e.g., Hartmann et al. 1984, Fritsch et al. 1986, Houze 1989, 2004, Donner et al. 2001, Del Genio and Kovari 2002, Schumacher et al. 2004, Nesbitt et al. 2006, Storelvmo 2012), nearly all climate models fail to represent mesoscale convective organization (Del Genio 2012), while system evolution is not represented at all (Ovchinnikov et al. 2006). Recent advances in cumulus parameterization coupled with increasing model resolution have improved predictions, but even relatively higher-resolution models without parameterized deep convection have some persistent kinematic and microphysical biases (e.g., Blossey et al. 2007, Matsui et al. 2009, Luo et al. 2010, Lang et al. 2011, Varble et al. 2011, Fridlind et al. 2012, Hagos et al. 2014, Varble et al. 2014a-b, Fan et al. 2017, Stanford et al. 2017, Han et al. 2019). To improve representation of convective systems in models requires adequate characterization of their predictability as a function of environmental conditions. Because of the significant sensitivities of deep convective initiation, intensity, lifetime, propagation, and mesoscale convective organization to many factors including multi-scale atmospheric circulations, ambient environmental stability, humidity, wind distributions, and cloud microphysical processes, this characterization relies on comprehensively observing many cases of convective initiation, non-initiation, organization, and non-organization.

The U.S. Department of Energy (DOE) Atmospheric Radiation Measurement (ARM) user facility's Cloud, Aerosol, and Complex Terrain Interactions (CACTI) experiment in the Sierras de Córdoba mountain range of north-central Argentina was designed to improve understanding of cloud life cycle and organization in relation to environmental conditions so that cumulus, microphysics, and aerosol parameterizations in multi-scale models can be improved. The Sierras de Córdoba range has a high frequency of orographic boundary-layer clouds, many reaching congestus depths, many initiating into deep convection, and some organizing into mesoscale systems uniquely observable from a single fixed site (Anabor et al. 2008, Romatschke and Houze 2010, Rasmussen and Houze 2011, Rasmussen et al. 2014, 2016, Rasmussen and Houze 2016). Some systems even grow upscale to become among the deepest, largest, and longest-lived in the world (Velasco and Fritsch 1987, Zipser et al. 2006, Salio et al. 2007, Durkee and Mote 2009, Durkee et al. 2009). These systems likely contribute to an observed regional trend of increasing extreme rainfall, and poor prediction of them likely contributes to a warm, dry bias in climate models downstream of the Sierras de Córdoba range (Carril et al. 2012, Solman et al. 2013) in a key agricultural region for the world.

Many environmental factors influence the convective life cycle in this region including orographic, low-level jet, frontal, and Andes-influenced synoptic-scale circulations (e.g., Salio et al. 2007, Borque et al. 2010, Nicolini and Skabar 2011), surface fluxes, cloud detrainment, and aerosol properties. Local and long-range transport of smoke resulting from biomass burning as well as blowing dust are common in the austral spring (e.g., Freitas et al. 2005, Winker et al. 2013, Camponogara et al. 2014), while changes in land surface properties as the wet season progresses impact surface fluxes and boundary-layer evolution on daily and seasonal time scales that feed back to cloud and rainfall generation (e.g., Sörensson and Menéndez 2011, Ruscica et al. 2015). This range of environmental conditions and cloud properties coupled with a high frequency of events makes this an ideal location for improving our understanding of cloud-environment interactions.

The following primary science questions are being addressed through coordinated first ARM Mobile Facility (AMF1), C-band Scanning ARM Precipitation Radar (C-SAPR2), ARM Aerial Facility (AAF) Gulfstream-1 (G-1) and guest instrument observations that were collected:

1. How are the properties and life cycles of orographically generated cumulus humulis, mediocris, and congestus clouds affected by environmental kinematics, thermodynamics, aerosols, and surface properties? How do these cloud types alter these environmental conditions?
2. How do environmental kinematics, thermodynamics, and aerosols impact deep convective initiation, upscale growth, and mesoscale organization? How are soil moisture, surface fluxes, and aerosol properties altered by deep convective precipitation events and seasonal accumulation of precipitation?

This multi-faceted experiment involved a long-term, 6.5-month, Extended Operational Period (EOP, 15 October 2018-30 April 2019) as well as a 1.5-month Intensive Operational Period (IOP, 30 October-13 December) that included G-1 flights and the multi-agency, National Science Foundation (NSF)-led, Remote sensing of Electrification, Lightning, And Mesoscale/microscale Processes with Adaptive Ground Observations (RELAMPAGO) field campaign.

Ground instrumentation deployed for CACTI is shown in Table 1 with primary measurements collected and known periods of bad or missing data. Aerosol observing system mentors worked on instruments from October 18-22 and on April 22. Data on these days should be used with caution. The 3-channel microwave radiometer failed to collect data, and the microwave radiometer profiler calibration is incorrect, rendering retrievals currently unusable. Because of the sheer volume of data collected, much of it has not been reviewed closely. Therefore, data users are encouraged to contact instrument mentors listed on the ARM website (www.arm.gov) with any questions.

Table 1. Ground instrumentation deployed for CACTI, the primary measurements or retrievals provided by instrumentation, and known periods with data quality issues. Measurements are colored by category where blue represents clouds/precipitation, green represents meteorological state, orange represents surface conditions, purple represents radiative fluxes, and maroon represents aerosols/trace gases.

Instrument	Measurements	Data Quality Issues
C-Band Scanning ARM Precipitation Radar 2 (C-SAPR2)	Precipitation kinematics and microphysics	No data from Dec 27-Jan 20, Feb 9-21, and Mar 3-6. From Mar 8-Apr 30, scans were limited to continuous W-E HSRHIs.
X-Band Scanning ARM Cloud Radar (X-SACR)	Precipitation kinematics and microphysics	No data from Jan 13-15 and Feb 18-23. Periods of no data from Apr 12-30. Scan strategy changed on Mar 8.
Ka-Band Scanning ARM Cloud Radar (Ka-SACR)	Cloud and precipitation kinematics and microphysics	Debris in transmitter caused variable loss of sensitivity; b1 data will have a calibration applied. Scan strategy changed on Mar 8.
Ka-Band ARM Zenith Radar (KAZR)	Cloud and precipitation kinematics and microphysics	21 days with 1-13-hour periods of no data caused by power loss and failure of UPS.
ARM cloud digital cameras (PI David Romps)	Cloud boundary locations	No data from Nov 5-20. Time drift on 1 camera requires correction. Limited cases being processed.
Total sky imager	Cloud fraction	2 short periods in Nov with no data.

Instrument	Measurements	Data Quality Issues
Parsivel Disdrometer	Precipitation size and fall speed distribution	
2-dimensional video disdrometer	Precipitation size, shape, and fall speed distribution	Periodic missing days from Jan 26-Apr 30.
Tipping bucket rain gauge	Precipitation rate	No data from Apr 1-10.
Pluvio-2 weighing bucket rain gauge	Precipitation rate	
Optical rain gauge	Precipitation rate	
Present weather detector	Precipitation rate	
Ceilometer	Cloud base; aerosol backscatter	
Micropulse lidar	Aerosol backscatter; cloud base	
Doppler lidar	Aerosol backscatter; boundary-layer horizontal and vertical winds; cloud base	
Radar wind profiler	Low tropospheric wind profile; precipitation kinematics and microphysics	Precipitation Doppler velocity is biased.
2-channel microwave radiometer	Column-integrated water vapor and liquid water	
High-frequency microwave radiometer	Column-integrated water vapor and liquid water	No data from Nov 27-Apr 30.
Meteorological station – M1 site	2-m pressure, temperature, humidity, and winds	Temperature and dew point may be high biased.
Meteorological station – S2 site	2-m pressure, temperature, humidity, and winds	No data from Oct 15-Nov 4. No wind data starting Nov 10.
Meteorological station – S3 site	2-m pressure, temperature, humidity, and winds	Periods of missing data from Oct 15-Nov 18. No data from Jan 21-Feb 28. No wind data starting Nov 10.
Aerosol observing system meteorological station	10-m pressure, temperature, humidity, and winds	RH is slightly low biased. Occasional erroneous spikes.
Mobile automated weather station	2-m pressure, temperature, humidity, and winds	No data from Dec 29-Jan 2.
Radiosonde – M1 site	Pressure, temperature, humidity, and wind profile	Near-surface temperature and dew point may be high biased.
Radiosonde – S1 site	Pressure, temperature, humidity, and wind profile	No data from Dec 19-Jan 7.
Sodar	Low-level wind profile	
Eddy correlation flux measurement systems	Surface turbulent fluxes of momentum, heat, moisture, and CO_2	Bad water vapor and CO_2 flux data from Jan 2-Feb 2.
Surface energy balance system	Soil temperature, moisture, and heat flux; upwelling and downwelling irradiance	Bad soil moisture data from Oct 15-23. No downward shortwave, surface energy balance, or albedo data from Oct 30-Feb 2.
Infrared thermometer – ground	Upwelling longwave narrowband brightness temperature; surface skin temperature	
Infrared thermometer – sky	Downwelling longwave narrowband brightness temperature	
Atmospheric emitted radiation interferometer	Downwelling longwave spectral radiance	
Ground radiation radiometers	Longwave and shortwave upwelling broadband irradiances	

Instrument	Measurements	Data Quality Issues
Sky radiation radiometers	Longwave and shortwave downwelling broadband irradiances	Bad data from Feb 23-25.
Hemispheric shortwave array spectroradiometer	Shortwave diffuse, direct, and normal spectral irradiance	
Zenith shortwave array spectroradiometer	Shortwave zenith spectral irradiance	No near-IR data collected.
Multifilter radiometer	Upwelling shortwave narrowband irradiance	No data from Oct 15-Nov 13.
Cimel sun photometer	Downwelling shortwave narrowband radiance; aerosol optical depth	Not yet processed.
Multifilter rotating shadowband radiometer	Downwelling shortwave narrowband irradiance; aerosol optical depth	
Condensation particle counter	Condensation nuclei (CN) concentration > 10 nm diameters	Bad data on Nov 1 and Jan 17-29.
Ultrafine condensation particle counter	CN concentration > 3 nm diameters	Bad data on Oct 15-20, Nov 1, Nov 4-6, and Jan 17-28. Flow rate issue from Feb 13-21.
Dual-column cloud condensation nuclei (CCN) counter	CCN at multiple supersaturations	Bad data on Nov 1, Feb 11-12, Mar 11-12, and Apr 1-8.
Aerosol chemistry speciation monitor	Aerosol chemical composition	Bad data on Oct 15-20 and Nov 8-12. Missing data from Jan 25-Apr 23.
Single-particle soot photometer	Black carbon concentration	Data collection ended Feb 26. Not yet processed.
Particle soot absorption photometer	Aerosol absorption and extinction	Bad data on Nov 1, Nov 16-20, and Mar 28.
Nephelometer – ambient	Aerosol scattering	Bad data on Nov 1 and Mar 28.
Nephelometer – variable relative humidity	Aerosol scattering	Bad data on Nov 1 and Mar 28.
Scanning mobility particle sizer (SMPS)	Aerosol size distribution (10-500 nm)	No data from Oct 26-27 and Oct 30-Nov 1. Offline for periods between Nov 2 and 13. Concentration spikes at intervals of 60-70 seconds and greater particle count uncertainty than typical from Oct 15-Nov 13.
Ultra-high-sensitivity aerosol spectrometer	Aerosol size distribution (60-1000 nm)	Bad data on Nov 1.
Aerodynamic particle sizer	Aerosol size distribution (500-20,000 nm)	Bad data on Oct 15-20, Nov 1, Dec 30-Jan 1, Jan 5, Jan 9, Mar 5, and Apr 15-30. Questionable data on several other days in Jan-Mar due to breakdown of laser voltage.
Ozone	Concentration	
Carbon monoxide, nitrous oxide, water vapor	Concentration	Bad data on Oct 31, Nov 2, and Jan 27-Feb 26.
Ice nucleating particle filters (PI Paul DeMott)	Temperature-dependent ice nucleating particle concentration	Processing in progress.

A map of the CACTI instrumentation sites is provided in Figure 1. Most instrumentation was deployed at the AMF1 site including the C-SAPR2. A site to the west of the mountains at Villa Dolores had a deployed meteorological station, and radiosondes were launched at least twice per day at 9 AM (12 UTC) and 3 PM (18 UTC). Soundings at the AMF1 site were launched every 3 or 4 hours between 9 AM and 9 PM (00 UTC) depending on whether deep convection was expected on a day or not. Two supplemental meteorological stations (automated weather stations; AWS) owned by ARM were deployed at higher elevations between the two sounding sites. Photogrammetric cameras (ACDC) were also deployed at two locations slightly offset from the AMF1 site with a 70º field of view (FOV) from SSW to just north of W. SACR RHIs in the 30-degree sector from WSW to W were also performed within this FOV targeting growing convective clouds. The AMF1 site was unique in that it was located on the eastern slope of the Sierras de Córdoba mountain range, but radar beam blockage was minimal (apart from the lowest levels to the west where the higher terrain was located). It was also mostly free of anthropogenic aerosol sources to the NE where the prevailing flow originated. A view toward the west at the AMF1 site is shown in Figure 2 along with views from the G-1 aircraft, showcasing the relatively open fields and pastures in the area.

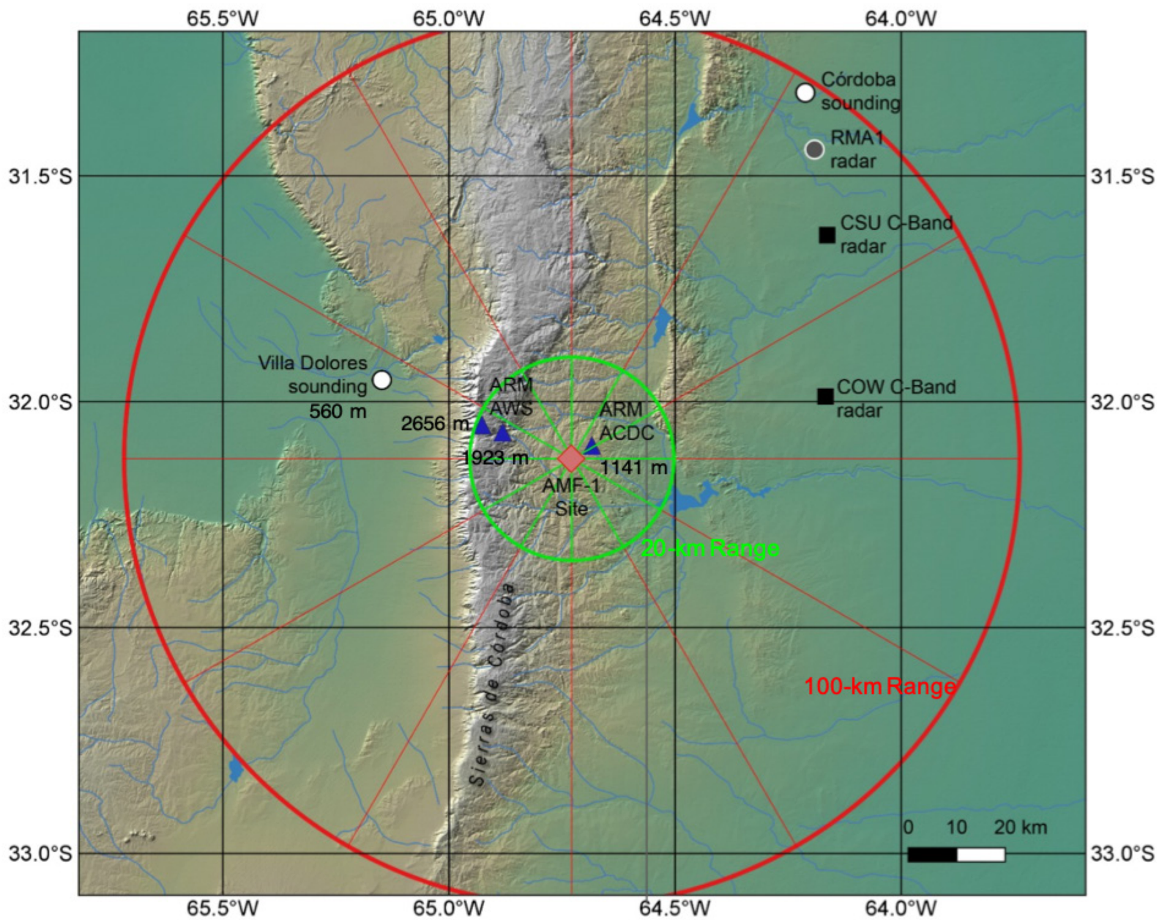

Figure 1. A map of the CACTI observing domain highlighting the Sierras de Córdoba mountain range, the AMF1 central site, nearby photogrammetric cameras (ACDC), upper-elevation meteorological stations, and the second sounding site at Villa Dolores. Hemispheric RHIs were performed by the scanning radars along with radials shown. The Argentinian operational RMA1 C-band radar and Córdoba sounding sites are also shown along with the NSF-led RELAMPAGO field campaign C-band radar locations.

Figure 2. A view west across the AMF1 site toward the crest of the Sierras de Córdoba mountain range (top; courtesy of Jason Tomlinson). Aerial views of the AMF1 site with surrounding land cover looking toward the east-southeast (bottom left; courtesy of Adam Varble) and zoomed in on the site with directions shown (bottom right; courtesy of Paloma Borque).

The idealized ground measurement strategy is shown in Figure 2 with typical daytime orographic upslope flows and occasional low-level jets that would bring in moisture from the Amazon. The most typical orographic cumulus clouds would form to the west of the AMF1 site, commonly advecting from north to south in a north-south oriented cloud line along the highest terrain. Free tropospheric flow nearly always had a westerly component, which would cause congestus clouds to shear toward the AMF1 site, as shown in Figure 2. Although convective clouds could be fed by air from both the west and east sides of the mountain range, the most typical situation involved clouds forming just east of the highest terrain being primarily fed by air originating on the east side of the terrain when clouds were coupled with the boundary layer. In these situations, the primary goal was to measure the properties of the air flowing upslope through the cloud bases while retrieving cloud properties and properties of detrained air aloft through remote sensing, radiosondes, and the G-1 aircraft at the same time.

CACTI employed a unique radar scan strategy. The C-SAPR2 performed a 15-tilt plan position indicator (PPI) "volume" between elevation angles of 0.5º and 33º followed by a ZPPI, a 6-azimuth hemispheric range-height indicator (HSRHI) pattern along the radials shown in Figures 1 and 3, followed by a repeat of the HSRHI pattern. This sequence was performed every 15 minutes. There were some events during the IOP period in which the HSRHI patterns were replaced with limited-sector RHIs targeting convective cells offset from the site. This was possible because the radar was operated in person by Joseph Hardin, Nitin Bharadwaj, Andrei Lindenmaier, Pete Argay, and Todd Houchens during the IOP. The X/Ka-SACR also had a 15-minute sequence but performed a 30º sector RHI scan between west-southwest and west followed by the previously described HSRHI pattern repeated three times in a row. The C-SAPR2 had pedestal issues that began in late December, resulting in periods with no data. In early March, the azimuthal pedestal became unrepairable on site. Therefore, at this time, the PI in consultation with the ARM radar team decided to scan the C-SAPR2 in a west-east HSRHI pattern for the rest of the campaign. To provide sufficient surveillance of nearby precipitation, the X/Ka-SACR then began performing PPI "volumes", which replaced the sector RHI and 1 of the HSRHI patterns in each 15-minute sequence. These volumes had a shorter range and lesser resolution than the C-SAPR2 volumes with greater attenuation at the higher frequencies, but overall, the switch worked well and the SACR continued to operate well for the majority of the field campaign.

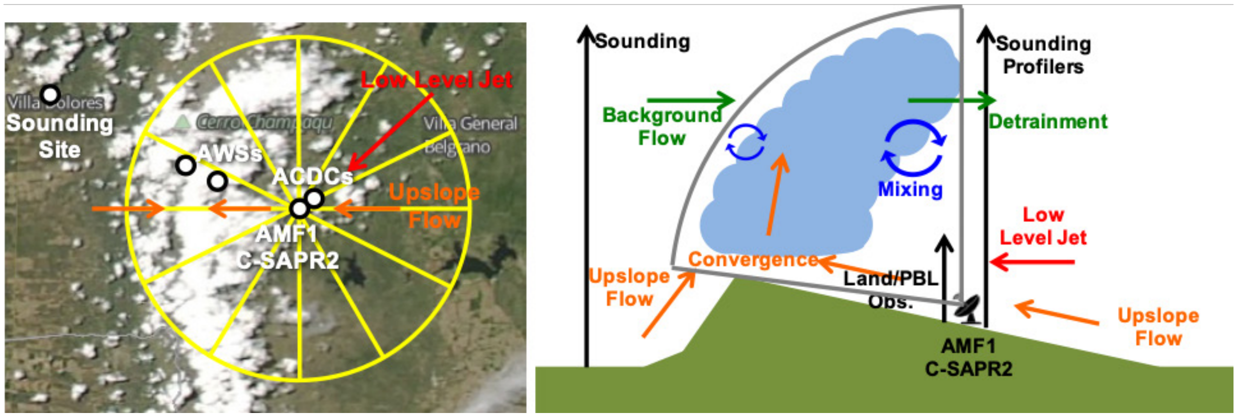

Figure 3. An idealized view of the CACTI measurement strategy showing typical flows and orographic cloud locations. The yellow circle and spokes represent the approximate range of the SACR and directions of HSRHIs.

The G-1 completed 22 flights during CACTI, totaling 79.4 hours of flight time. Each flight is described in Table 2. Instrumentation installed on the G-1 is shown in Table 3 with measurements made and known data quality issues. The F-FSSP probe was also flown on the G-1 but the probe failed to collect useable data. While in cloud, aerosols were sample from cloud droplet residuals provided by the counterflow virtual impactor. Most flights performed north-south, constant altitude legs over the AMF site, over the highest terrain where clouds were most frequent, and to the west of the clouds and highest terrain (see Figure 4). Legs were flown just below cloud base when possible, at mid-cloud level, and at cloud top, repeating in time. Some flights included a spiral down over the AMF site to provide an aerosol and thermodynamic profile. Deviations from this strategy were performed when a situation dictated it. For example, if it seemed that clouds were primarily ingesting cloud base air from the west of the mountains, a leg was flown in the boundary layer west of the mountains. When radiosondes were launched or deep convective precipitation formed, those areas were avoided.

Table 2. CACTI G-1 flights including their date, time period, and primary target.

Flight	Time	Target
1	13:02-17:01 UTC Nov 4	Deepening orographic cumulus clouds
2	13:09-17:05 UTC Nov 6	Deep convective initiation; warm rain likely present
3	12:10-16:10 UTC Nov 10	Deepening orographic cumulus clouds pre-deep convective initiation
4	16:48-20:00 UTC Nov 12	Elevated deep convection; cumulus and stratus in stable low levels
5	14:00-18:00 UTC Nov 14	Clear-air aerosol sampling
6	13:05-16:00 UTC Nov 15	Clear-air aerosol sampling
7	14:05-18:00 UTC Nov 16	Boundary layer and elevated orographic cumulus layers

Flight	Time	Target
8	12:18-16:30 UTC Nov 17	Congestus cloud line along cold front; wind-blown dust; mountain wave present
9	15:10-19:06 UTC Nov 20	Orographic cumulus and strong inversion
10	18:22-20:27 UTC Nov 21	Orographic congestus and deep convective initiation
11	14:31-18:11 UTC Nov 22	Stratiform and anvil sampling on back side of exiting MCS along radar N-S scans
12	16:17-20:25 UTC Nov 24	Orographic cumulus congestus line with strong inversion
13	15:51-19:07 UTC Nov 25	Orographic cumulus line; potentially decoupled from boundary layer
14	15:08-18:50 UTC Nov 28	Orographic congestus fed from air to the west; deep convective initiation late in flight
15	14:16-16:32 UTC Nov 29	Orographic congestus initiating into deep convection
16	16:20-18:47 UTC Dec 1	Elevated drizzling clouds; possibly ice near -10C cloud tops
17	12:06-16:11 UTC Dec 2	Elevated drizzle; unclear whether ice was present
18	16:03-20:09 UTC Dec 3	Boundary-layer coupled orographic cumulus in strong inversion
19	17:51-19:45 UTC Dec 4	Deepening congestus clouds, some initiating into deep convection
20	12:04-15:28 UTC Dec 5	Mid-level cloud deck seen by KAZR; deepening congestus that initiated into deep convection
21	15:01-19:01 UTC Dec 7	Orographic cumulus with strengthening inversion
22	16:06-19:30 UTC Dec 8	Clear-air aerosol sampling

Figure 4. A map overlaid with the flight tracks from all 22 flights (left; courtesy of Alyssa Matthews) showing the location of the airport in Rio Cuarto and the AMF1 site. The upper right picture (courtesy of Jason Tomlinson) is from an outreach event and the lower right picture (courtesy of Adam Varble) shows cumulus congestus from Flight 10 with ice forming in one of the turrets.

Table 3. G-1 aircraft instrumentation during CACTI with primary measurements of each instrument and known data quality issues.

Instrument	Measurements	Data Quality Issues
Isokinetic inlet	Heated inlet for sampling clear air	
Counterflow virtual impactor with LICOR-840A	Inlet for sampling cloudy air residuals	
Water content meter-2000	Total, liquid, and inferred ice water content	
Particle volume monitor-100A	Liquid water content	
Hotwire on CAPS	Liquid water content	
Cloud particle imager	Single cloud particle images	No data on Nov 14-15.
Fast-cloud droplet probe	10 Hz cloud droplet size distribution (2-50 μm)	
2-dimensional stereo probe	Cloud droplet size distribution (10-3000 μm)	
Cloud imaging probe	Cloud droplet size distribution (25-1500 μm)	
High-volume precipitation spectrometer 3	Cloud droplet size distribution (150-19,600 μm)	
SMPS	Aerosol size distribution (10-500 nm)	Bad data on Nov 25.
Ultra-high-sensitivity aerosol spectrometer	Aerosol size distribution (60-1000 nm)	Missing data for last hour of flight on Nov 10.
Passive cavity aerosol spectrometer	Aerosol size distribution (100-3000 nm)	Use data on Nov 24-25 with caution.
Optical particle counter	Aerosol size distribution (700-15,000 nm)	
Cloud aerosol spectrometer – dual polarized	Aerosol size distribution (500-50,000 nm)	
Dual-column CCN counter	CCN concentration at 2 supersaturations	Bad data on Nov 4 and 6.
Condensation particle counter	CN concentration > 10 nm diameters	Use data on Nov 4 and 6 with caution.
Ultrafine condensation particle counter	CN concentration > 3 nm diameters	Use data on Nov 4 and 6 with caution.
3-wavelength integrating nephelometer	Aerosol scattering	
3-wavelength single-channel tricolor absorption photometer	Aerosol absorption	
Particle soot absorption photometer	Aerosol absorption and extinction	
Single-particle soot photometer	black carbon concentration	
Ice nucleating particle filters	Temperature-dependent ice nucleating particle concentration	Currently processing. No filters collected Nov 4.
Single-particle mass spectrometer (Mini-SPLAT II) (PI Alla Zelenyuk-Imre)	Aerosol chemical composition	Currently processing.
Ozone	Concentration	
Sulfur dioxide	Concentration	
Carbon monoxide, nitrous oxide, water vapor	Concentration	
Aircraft Integrated Meteorological Measurement System (AIMMS-20)	5-port air motion: true airspeed, angle-of-attack, sideslip position, velocity, attitude temperature and relative humidity	From Nov 17 onward, sampling decreased from 20 to 5 Hz.

Instrument	Measurements	Data Quality Issues
Interagency Working Group for Airborne Data and Telemetry Systems (IWGADTS) suite	Combines AIMMS-20, C-MIGITS, DSM, Rosemount E102AL (temperature), GE-1011B chilled hygrometer (dew point temperature), and Rosemount 1201F1 (static pressure)	
GE-1011B chilled-mirror hygrometer	Dew point temperature	
Tunable diode laser hygrometer	20 Hz absolute humidity	
Reverse-flow temperature probe	100 Hz temperature	Not processed
Gust probe: Rosemount 1221F2	100 Hz 5-port air motion: pressures, accelerations, temperature	
C-MIGITS III GPS/INS	10 Hz position, velocity, attitude	
GPS DSM 232	Position, velocity	
VectorNav-200 GPS/INS	40 Hz position, velocity, attitude	
Video camera P1344	Forward video images	

CACTI coincided with a NSF-led field campaign called RELAMPAGO (Remote sensing of Electrification, Lightning, And Mesoscale/microscale Processes with Adaptive Ground Observations; PI Steve Nesbitt, University of Illinois), which included a hydrologic component from June 2018 through April 2019 (PIs Francina Dominguez [University of Illinois], David Gochis (National Center for Atmospheric Research], and Marcelo Garcia [University of Córdoba]) and an IOP between November 2018 and January 2019 (Figure 5). Primary goals of RELAMPAGO included bettering understanding of deep convective initiation, upscale growth, severe weather, lightning, and hydrologic processes within the context of the high societal impacts they produce. RELAMPAGO and CACTI teams coordinated with one another during the IOP period because of their shared interest in targeting initiating and growing deep convective clouds.

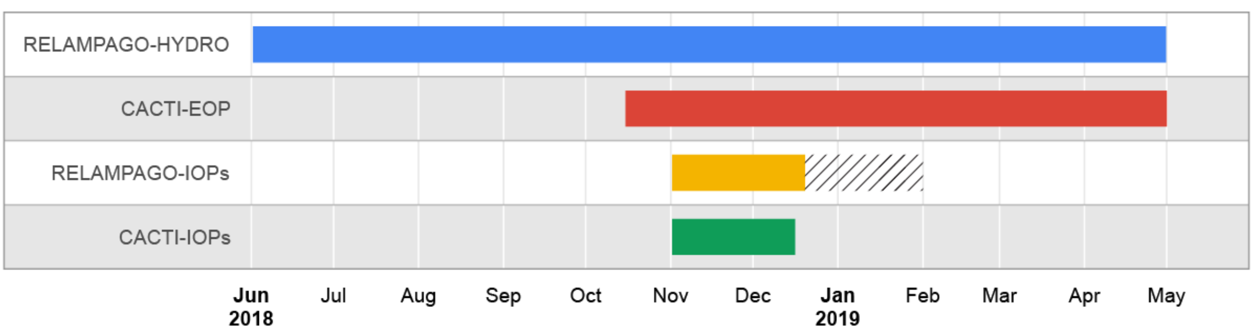

Figure 5. The CACTI extended operational period and IOP within the context of the RELAMPAGO-Hydro and IOP timelines. The hatch shading indicates a period in which the CSU C-band radar continued making measurements and extra SMN radiosondes were launched in Córdoba.

RELAMPAGO-Hydro deployed 15 National Center for Atmospheric Research (NCAR) Earth Observing Laboratory (EOL) surface stations across the region (4 within the CACTI observing area) that each included measurements of pressure, temperature, humidity, winds, precipitation, soil moisture, temperature, heat flux, heat capacity, leaf wetness, and incoming/outgoing shortwave and longwave radiation. A subset of stations also included surface flux and Parsivel disdrometer measurements. Fifteen NCAR Research Applications Laboratory (RAL) stations were also deployed across the region (seven within with CACTI observing area) with measurements of pressure, temperature, humidity, winds, precipitation, soil temperature and moisture, leaf wetness, and downwelling shortwave radiation. Five streamflow gauges were also observed within the CACTI observing area. These data sets should be available in early 2020 from the RELAMPAGO EOL website (https://www.eol.ucar.edu/field_projects/relampago).

The RELAMPAGO IOP period enveloped with the CACTI IOP and included deployment of a wide range of fixed and mobile instrumentation within the CACTI observing area. Two fixed C-band radars were installed (Figure 1) on the plains to the east of the Sierras de Córdoba mountain range. The Colorado State University (CSU) C-band radar began operation on November 10, 2018 and operated through January 31, 2019 using a mixture of PPI and RHI patterns on a 10-minute heartbeat that depended on the targeted phenomena. The Center for Severe Weather Research (CSWR) C-band on Wheels (COW) radar was operated for IOPs 7-17 (see Table 4). A micropulse differential absorption lidar was deployed east of the CSU C-band radar to retrieve continuous water vapor profiles. Lightning mapping arrays and electric field mills from multiple institutions/agencies were also deployed. Mobile instrumentation was deployed for the IOPs in Table 4 (see http://catalog.eol.ucar.edu/relampago/tools/missions for more details). It included 3 CSWR Doppler on Wheels (DOW) X-band radars, 6 mobile radiosonde vehicles (3 CSWR, 2 University of Illinois at Urbana-Champaign [UIUC], 1 CSU), CSWR deployable meteorological stations (Pods) and disdrometers, and 6 CSWR mobile mesonets. Some Argentinean observations will also be provided through the RELAMPAGO EOL website including Servicio Meteorológico Nacional (SMN) operational C-band radar and radiosonde measurements from Córdoba (see Figure 1), as well as regional meteorological and hydrological networks. RELAMPAGO data sets will be available in early 2020.

Table 4. RELAMPAGO IOP time periods, mission type, and mobile instrumentation involved including the DOWs, Pods, and disdrometers from CSWR, and radiosondes from CSWR, UIUC, and CSU.

IOP	Date/Time	Mission Type	Mobile Instrumentation
1	18Z Nov 2-00Z Nov 3	Convective initiation	Soundings: CSU, 2 UIUC, 3 CSWR Radar: DOW6, DOW7, DOW8
2	09Z-18Z Nov 5	Upscale growth	Soundings: CSU, 2 UIUC, 3 CSWR Radar: DOW7, DOW8
3	12Z-21Z Nov 6	Convective initiation	Soundings: CSU, 2 UIUC, 3 CSWR Radar: DOW7, DOW8
4	15Z-22Z Nov 10	Severe weather	Soundings: CSU, 2 UIUC, 3 CSWR Radar: DOW6, DOW7, DOW8
5	00Z-09Z Nov 12	Upscale growth	Soundings: CSU, 2 UIUC, 3 CSWR Radar: DOW6, DOW7, DOW8
6	08Z-14Z Nov 17	Special: joint mission	Soundings: CSU, 2 UIUC, 3 CSWR
7	15Z-21Z Nov 21	convective initiation	Soundings: CSU, 2 UIUC, 3 CSWR Radar: DOW6, DOW7, DOW8
8	14Z-20Z Nov 22	Severe weather (upscale growth handoff)	Soundings: CSU, 2 UIUC, 3 CSWR Radar: DOW6, DOW7, DOW8
9	14Z-20Z Nov 25	Severe weather (San Rafael)	Soundings: CSU, 2 UIUC, 3 CSWR Radar: DOW6, DOW7, DOW8
9B	00Z-18Z Nov 26	Special: upscale growth	Fixed instrumentation only

IOP	Date/Time	Mission Type	Mobile Instrumentation
10	13Z-20Z Nov 26	Convective initiation (San Rafael)	Soundings: CSU, 2 UIUC, 3 CSWR Radar: DOW7, DOW8
11	13Z-20Z Nov 29	Convective initiation (upscale growth handoff)	Soundings: CSU, 2 UIUC, 3 CSWR Radar: DOW7, DOW8
12	14Z-22Z Nov 30	Upscale growth	Soundings: CSU, 2 UIUC, 3 CSWR Radar: DOW7, DOW8
13	14Z-20Z Dec 4	Convective initiation (severe handoff)	Soundings: CSU, 2 UIUC, 3 CSWR Radar: DOW6, DOW7, DOW8
14	14Z-22Z Dec 5	Upscale growth	Soundings: CSU, 2 UIUC, 3 CSWR Radar: DOW7, DOW8
15	17Z-21Z Dec 10	Severe weather	Soundings: CSU, 2 UIUC, 3 CSWR Radar: DOW6, DOW7, DOW8
16	17Z-22Z Dec 11	Severe weather	Soundings: CSU, 2 UIUC, 3 CSWR Radar: DOW6, DOW7, DOW8
17	22Z Dec 13-03Z Dec 14	Upscale growth (severe secondary)	Soundings: CSU, 2 UIUC, 3 CSWR Radar: DOW7, DOW8
18	19Z-23Z Dec 15	Special: water vapor transport study	Soundings: 2 UIUC, 3 CSWR Radar: DOW7, DOW8
19	16Z-21Z Dec 16	Convective initiation	Soundings: 2 UIUC, 3 CSWR Radar: DOW7

Many unique events were observed during CACTI — some that were anticipated and others that were not. As was expected, many cases involved orographic clouds tied to the terrain that slowly deepened over time and initiated into deep convection within close proximity of the AMF1 site. Also as expected, hail was frequently observed, and the deepest convective cells penetrated above 20 km above sea level. Less expected was the high frequency of elevated convection decoupled from the surface, commonly resulting in warm rain, an example of which is shown in Figure 6 from vertically pointing KAZR and scanning Ka-SACR perspectives. Clean periods with almost no CCN were also observed during and after periods of significant rainfall, an example of which is shown in Figure 7. This frequently led to fog. Orographic cumulus clouds also frequently expanded horizontally in time such that they could accurately be called stratocumulus cloud decks confined to the higher terrain. Aerosol size distributions significantly varied in time with many days suggestive of new particle formation and growth, as seen in Figure 7.

CACTI was also unique in that it included the first C-SAPR2 deployment, which coincided with the collection of some of the best radar data sets ever collected by ARM. The lengthy hemispheric RHI (HSRHI) data set at Ka-, X-, and C-bands is one of a kind. An example of X-SACR HSRHIs at two different azimuths during a period of initiating deep convection is shown in Figure 8, highlighting fine-scale kinematic and microphysical properties of precipitation cores and convective circulations. In addition, GOES-16 mesoscale domain sectors were requested and granted by the National Oceanic and Atmospheric Administration (NOAA) for most of the deep convective events observed, which means that 1-minute satellite data is available for a large number of convective events that can be coupled with the detailed data collected on the ground and by aircraft during CACTI.

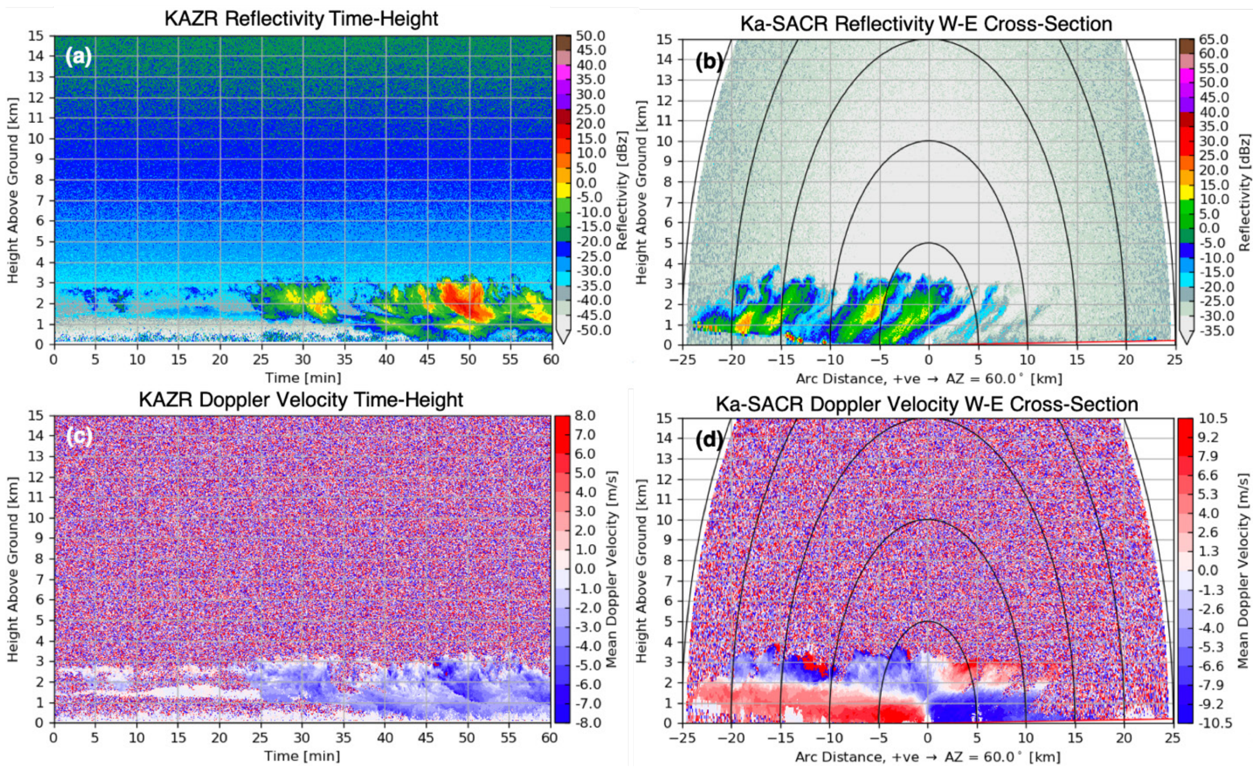

Figure 6. (a) KAZR reflectivity over a 1-hour period with (b) Ka-SACR reflectivity in a west-east HSRHI cross-section at one time during the hour. Mean Doppler velocity from the two radars are shown in (c) and (d), respectively, highlighting shallow convection near cloud top in (c) and surface-decoupled westerly component flow layer in which the precipitation is forming above upslope easterly component flow. Images are courtesy of Joseph Hardin and Nitin Bharadwaj.

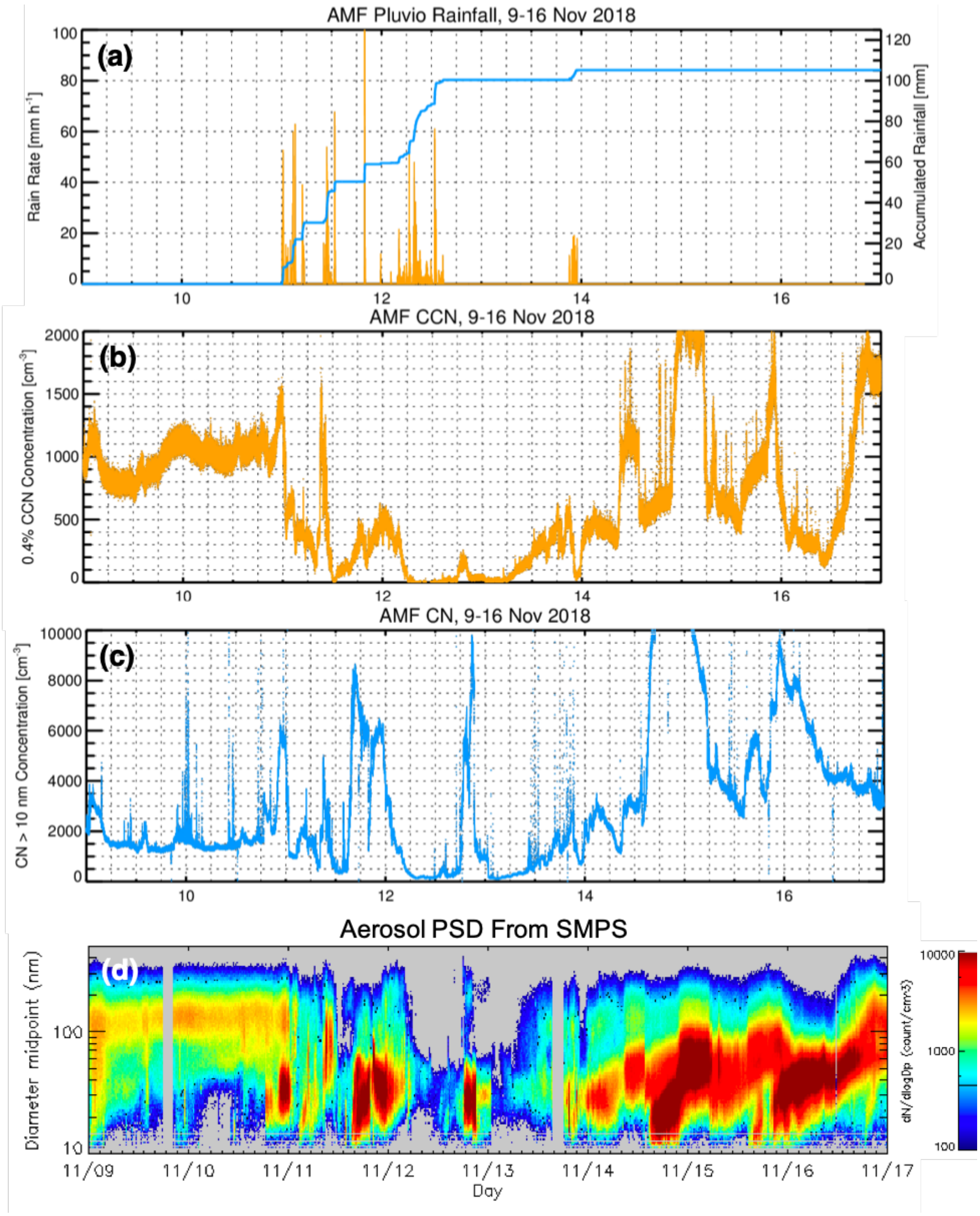

Figure 7. A 7-day period in November 2018 showing AMF1 site (a) Pluvio-2 rain rate and accumulated rainfall, (b) 0.4% supersaturation CCN, (c) CN > 10 nm diameter concentration, and (d) aerosol size distribution from the SMPS (panel (d) courtesy of the ARM Data Quality Office). This period showcases the significant variability in aerosol concentrations and sizes affected by wet sedimentation and new particle formation and growth events.

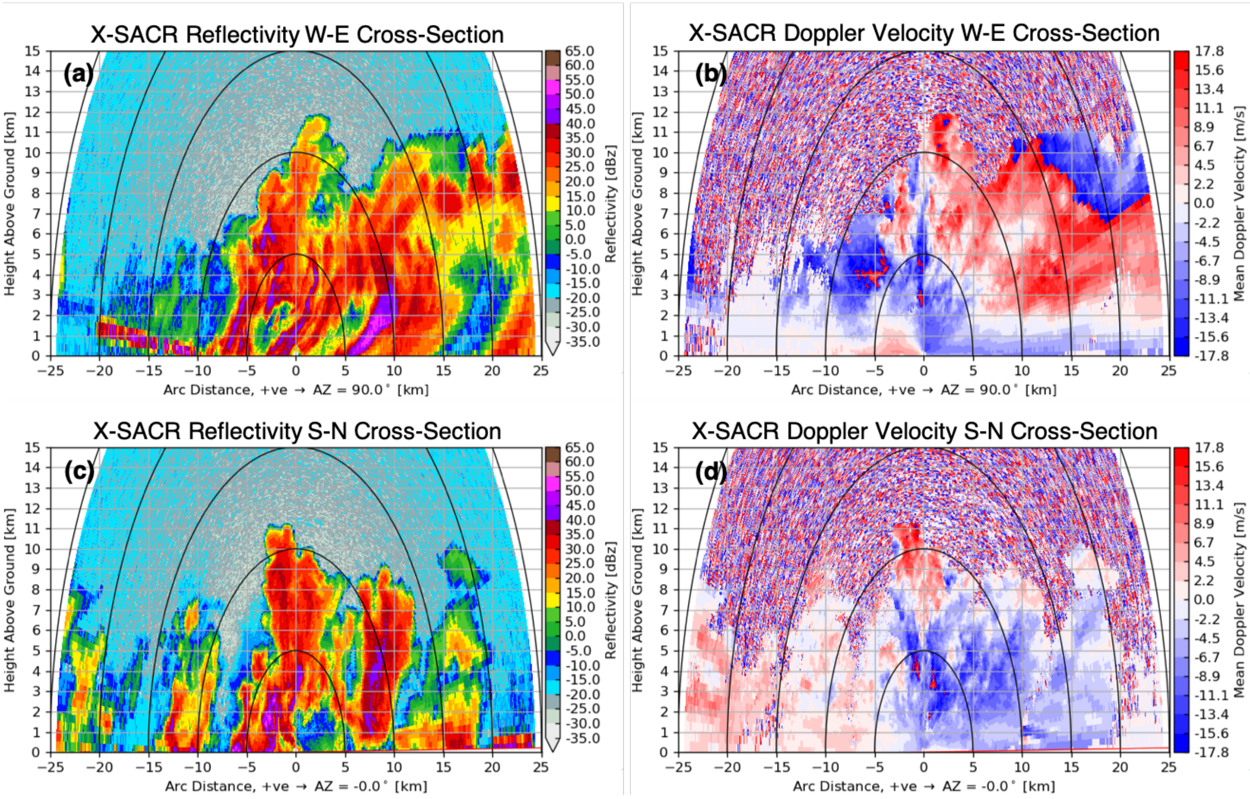

Figure 8. Example HSRHIs from the X-SACR during a deep convective initiation and growth event showing (a-b) west-east cross-sections of reflectivity and mean Doppler velocity and (c-d) south-north cross-sections of the same variable where 0 is the location of the radar at the AMF1 site. Each HSRHI is separated in time by less than 2 minutes and HSRHIs were also performed at 4 additional azimuths. Images are courtesy of Joseph Hardin and Nitin Bharadwaj.

2.0 Results

All results are very preliminary with the focus having been on quality controlling data sets to get them ready for release by the end of the 2019 calendar year. Several principal investigator (PI) and value-added products have been completed while others are still being processed or planned (Table 5).

Table 5. DOE ARM value-added products planned for CACTI including their current/planned availability. PI products are also listed and include the PI name where possible.

VAP	Measurement	Availability
AERINF	Longwave spectral radiances	Planned for FY20
AOD	Aerosol optical depth	Planned for FY20
AOP	Aerosol optical properties	Processed
KAZR-ARSCL	Cloud boundary time-heights	Being processed
DLPROF	3-D wind profiles	Available
INTERPSONDE	Interpolated temperature, humidity, pressure, and wind time-heights	Being processed
MPLCLDMASK	Cloud mask and depolarization ratio from micropulse lidar	Available

MWRRET	Precipitable water vapor and liquid water path estimates	Planned for FY20
PBLHT	Boundary-layer height estimates	Being processed
QCECOR	Quality-controlled latent and sensible surface fluxes	Being processed
QCRAD	Quality-controlled surface radiative fluxes	Planned for FY20
RADFLUX	QCRAD with clear sky downwelling broadband radiation for computing CRE	Planned for FY20
MERGESONDE	Temperature, humidity, pressure, and wind time-heights including background ECMWF analyses	Planned for FY20
AERIoe	Boundary-layer temperature and humidity	Planned for FY20
ARMBE	Hourly best-estimated climate relevant variables	Planned for FY20
VARANAL	Large-scale advective tendencies	Planned for FY20
SatCORPS (Langley)	GOES-16 cloud retrievals at 1 or 15-min frequency depending on time period	Being processed
LDQUANTS	Derived radar variables from Parsivel disdrometer data	Available
Taranis (PI Joseph Hardin)	Radar corrections, masks, and hydrometeor retrievals for C-SAPR2 and X-SACR	Being processed
Cartesian Gridded C-SAPR2 Data	C-SAPR2 processed through Taranis and Cartesian gridded	Being processed
Cartesian Gridded SACR Data	Ka/X-SACR processed through Taranis and Cartesian gridded	Being processed
CMAC2.0	Radar corrections, masks, and hydrometeor retrievals	Planned for FY20
PCCPP (PI David Romps)	Cloud boundary locations and movements from stereo cameras	Being processed for select cases
Ice Nucleating Particle Concentrations (PI Paul DeMott)	Temperature-dependent ice nucleating particle concentrations	Being processed for select cases

Current work focuses on developing scanning radar data sets including retrievals such as rain rate that can be easily used by the research community. Work is also ongoing to identify and track convective cloud objects such that all such objects that pass over or near the AMF1 site are placed into life cycle context. Finally, experiment days are further being classified by phenomena observed building on the rough separations in Table 6. Ongoing research is focusing on many topics including:

- aerosol and cloud diurnal and seasonal cycles
- raindrop size distribution variability and relationships with convective cloud object properties
- convective cloud object microphysical and dynamical structures via HSRHIs
- wet deposition of aerosols
- precipitation impacts on surface fluxes and boundary-layer evolution
- meteorological and aerosol impacts on convective cloud properties
- cloud transport and processing of aerosols
- cloud dynamics and turbulence impacts on cloud droplet growth
- impacts of INP properties on primary ice nucleation in convective clouds
- warm rain formation processes
- shallow-to-deep convective transition processes
- links between convective updrafts, downdrafts, and cold pools
- mesoscale organization processes.

Table 6. CACTI days subjectively determined to have rainfall, deep convection, or cumulus/stratocumulus occur directly over the site using a combination of satellite, KAZR, and ceilometer data.

Cloud Regime over AMF Site	Dates
Cumulus humulis, congestus or stratocumulus (173 days)	October 16, 18, 19, 20, 21, 22, 23, 24, 25, 26, 27, 28, 29, 30 November 1, 2, 3, 4, 5, 6, 7, 8, 9, 10, 11, 12, 13, 15, 16, 17, 20, 21, 22, 23, 24, 25, 26, 27, 28, 29, 30 December 1, 2, 3, 4, 5, 6, 7, 9, 10, 11, 12, 13, 14, 16, 17, 18, 19, 20, 21, 22, 25, 26, 27, 28, 29, 31 January 1, 2, 3, 4, 5, 6, 7, 8, 9, 10, 11, 12, 13, 14, 15, 16, 18, 19, 20, 21, 22, 23, 24, 25, 27, 28, 29, 30, 31 February 1, 2, 3, 4, 5, 6, 7, 8, 9, 10, 11, 12, 13, 14, 15, 16, 17, 18, 19, 21, 22, 23, 24, 25, 26, 27 March 1, 3, 4, 5, 6, 7, 8, 9, 10, 11, 12, 13, 14, 15, 16, 17, 18, 19, 20, 21, 22, 24, 25, 26, 27, 28, 29, 30, 31 April 1, 2, 4, 10, 11, 13, 14, 15, 16, 17, 18, 19, 20, 21, 22, 23, 24, 25, 26, 27, 29, 30
Deep convection (79 days)	October 17, 18, 19, 22, 24, 25, 26, 28, 30, 31 November 3, 4, 5, 6, 10, 11, 12, 13, 17, 22, 26, 27, 29, 30 December 1, 2, 5, 6, 10, 13, 14, 18, 19, 20, 27, 28, 30 January 2, 3, 6, 9, 10, 13, 14, 15, 17, 22, 23, 24, 25, 26, 29, 30, 31 February 1, 8, 11, 12, 19, 21, 23, 24 March 4, 7, 8, 9, 15, 16, 17, 20, 25, 31 April 1, 15, 20, 21, 22, 24, 30
Surface rainfall (92 days)	October 17, 18, 19, 20, 22, 23, 24, 25, 26, 28, 30, 31 November 1, 3, 4, 5, 6, 7, 11, 12, 13, 22, 26, 27, 28, 29, 30 December 1, 2, 5, 10, 13, 14, 18, 19, 20, 27, 28, 30 January 2, 3, 6, 9, 10, 13, 14, 15, 17, 18, 22, 23, 25, 26, 29, 30, 31 February 1, 3, 8, 9, 11, 12, 22, 23, 24, 25, 26 March 4, 5, 8, 9, 11, 12, 14, 15, 16, 17, 19, 20, 26, 26, 31 April 1, 15, 20, 21, 22, 24, 25, 26, 27, 30

For many of these topics, research is extending to multi-scale model and parameterization evaluation. A Weather Research and Forecasting (WRF) run with 3-km horizontal grid spacing and aerosol-aware microphysics has already been run for the entire CACTI field campaign over an 1800 by 1500 km domain. This run has uniquely designed output targeting comparisons to high-time-resolution AMF1, C-SAPR2, and satellite measurements. Kilometer-scale and large-eddy simulations of well-observed shallow-to-deep convective cloud transition and mesoscale convective organization cases are also planned.

For a detailed list of additional research questions that could potentially be addressed with CACTI data sets, researchers are encouraged to consult Section 5 of the CACTI Science Plan (link provided in Section 3.1).

3.0 Publications and References

3.1 Journal Articles

No journal articles have been submitted or published yet with the campaign having ended 6 months ago. The science plan was published in August 2018:

Varble, AC, and the CACTI Science Team. 2018. Cloud, Aerosol, and Complex Terrain Interactions (CACTI) Science Plan. U.S. Department of Energy. DOE/SC-ARM-17-004, https://www.arm.gov/publications/programdocs/doe-sc-arm-17-004.pdf

3.2 Presentations

Preliminary results were shown in the following presentations:

Varble, AC, and the CACTI Science Team. 2019. "The Cloud, Aerosol, and Complex Terrain Interactions (CACTI) field campaign." Invited presentation at Pacific Northwest National Laboratory. Richland, Washington.

Varble, AC, and the CACTI Science Team. 2019. "The Cloud, Aerosol, and Complex Terrain Interactions (CACTI) field campaign." Invited presentation at the National Center for Atmospheric Research. Boulder, Colorado.

Collis, S, S Xie, S Giangrande, and S Tang. 2019. "CACTI VAPs Update." Presented at the ARM/ASR PI Meeting. Rockville, Maryland.

Hardin, J, N Bharadwaj, A Hunzinger, B Isom, A Lindenmaier, A Matthews, P Argay, and T Houchens. 2019. "Radar Status: CACTI/RELAMPAGO." Presented at the ARM/ASR PI Meeting. Rockville, Maryland.

Hardin, J., N Bharadwaj, S. Giangrande, A Varble, and Z Feng. 2019. "Taranis: Advanced Precipitation and Cloud Products for ARM Radars." Presented at the ARM/ASR PI Meeting. Rockville, Maryland.

Matthews, A, P Borque, P DeMott, L Goldberger, T Hill, F Mei, A Mendoza, D Nelson, M Newburn, M Pekour, B Schmid, A Sedlacek, S Springston, K Suski, J Tomlinson, A Varble, and A Zelenyuk-Imre. 2019. "Overview of the ARM Aerial Facility data during CACTI." Presented at the ARM/ASR PI Meeting. Rockville, Maryland.

Nesbitt, SW, AC Varble, and PC Borque. 2019. "Adaptive radar scanning in CACTI-RELAMPAGO." Presented at the ARM/ASR PI Meeting. Rockville, Maryland.

Varble, AC, and the CACTI Science Team. 2019. "The Cloud, Aerosol, and Complex Terrain Interactions (CACTI) field campaign." Invited presentation at the ARM/ASR PI Meeting. Rockville, Maryland.

Varble, AC, and the CACTI Science Team. 2019. "The Cloud, Aerosol, and Complex Terrain Interactions (CACTI) field campaign: Overview." Presented at the ARM/ASR PI Meeting. Rockville, Maryland.

Varble, AC, and the CACTI Science Team. 2019. “The Cloud, Aerosol, and Complex Terrain Interactions (CACTI) field campaign: LACI Measurements.” ARM/ASR PI Meeting. Rockville, Maryland.

Nesbitt, SW, and coauthors. 2019. “Mesoscale flows during convective initiation and upscale growth observed during RELAMPAGO-CACTI.” Invited keynote presentation at the AMS 18th Conference on Mesosocale Meteorology. Savanna, Georgia.

Schumacher, RS, DA Hence, NR Kelly, KA Kosiba, SW Nesbitt, RJ Trapp, and J Wurman. 2019. “High-Frequency Mobile Soundings in Convective Environments during RELAMPAGO: Overview and Preliminary Findings.” Presented at the AMS 18th Conference on Mesoscale Processes. Savannah, Georgia.

Singh, IT and SW Nesbitt. 2019. “High-resolution idealized simulations of orographic convection initiation over the Sierras de Córdoba Mountains.” Presented at the AMS 18th Conference on Mesoscale Processes. Savannah, Georgia.

Varble, AC, and the CACTI Science Team. 2019. “Data sets and Preliminary Results from the Cloud, Aerosol, and Complex Terrain Interactions (CACTI) field campaign.” Presented at the AMS 18th Conference on Mesoscale Processes. Savannah, Georgia.

Bharadwaj, N, J Hardin, S Giangrande, and A Varble. 2019. “Taranis: Advanced Precipitation and Cloud Radar Products.” Presented at the 39th International Conference on Radar Meteorology. Nara, Japan.

Isom, B, N Bharadwaj, and A Varble. 2019. “Exploring the Spatial Variability of Cloud Structures from the ARM CACTI Campaign.” Presented at the 39th International Conference on Radar Meteorology. Nara, Japan.

3.3 References

Anabor, V, DJ Stensrud, and OLL de Moraes. 2008. “Serial upstream-propagating mesoscale convective system events over southeastern South America.” *Monthly Weather Review* 136(8): 3087–3105, https://doi.org/10.1175/2007MWR2334.1

Blossey, PN, CS Bretherton, J Cetrone, and M Kharoutdinov. 2007. “Cloud-resolving model simulations of KWAJEX: Model sensitivities and comparisons with satellite and radar observations.” *Journal of the Atmospheric Sciences* 64(5): 1488–1508, https://doi.org/10.1175/JAS3982.1

Borque, P, P Salio, M Nicolini, and YG Skabar. 2010. “Environment associated with deep moist convection under SALLJ conditions: A case study.” *Weather and Forecasting* 25(3): 970–984, https://doi.org/10.1175/2010WAF2222352.1

Camponogara, G, MAF Silva Dias, and GG Carrio. 2014. “Relationship between Amazon biomass burning aerosols and rainfall over the La Plata Basin.” *Atmospheric Chemistry and Physics* 14(9): 4397–4407, https://doi.org/10.5194/acp-14-4397-2014

Carril, AF, CG Menendez, ARC Remedio, F Robledo, A Sorensson, B Tencer, J-P Boulanger, M d Castro, D Jacob, H Le Truet, LZX Li, O Penalba, S Pfeifer, M Rusticucci, P Salio, P Samuelsson, E Sanchez, and P Zaninelli, 2012. "Performance of a multi-RCM ensemble for South Eastern South America." *Climate Dynamics* 39(12): 2747–2768, https://doi.org/10.1007/s00382-012- 1573-z

Del Genio, AD, and W Kovari. 2002. "Climatic properties of tropical precipitating convection under varying environmental conditions." *Journal of Climate* 15(18): 2597–2615, https://doi,org/10.1175/1520-0442%282002%29015%3C2597%3ACPOTPC%3E2.0.CO%3B2

Del Genio, AD. 2012. "Representing the sensitivity of convective cloud systems to tropospheric humidity in general circulation models." *Surveys in Geophysics* 33(3–4): 637–656, https://doi.org/10.1007/s10712-011-9148-9

Del Genio, AD, J Wu, and Y Chen. 2012. "Characteristics of mesoscale organization in WRF simulations of convection during TWP-ICE." *Journal of Climate* 25(17): 5666–5688, https://doi.org/10.1175/JCLI-D-11-00422.1

Donner, LJ, CJ Seman, RS Hemler, and S Fan. 2001. "A cumulus parameterization including mass fluxes, convective vertical velocities, and mesoscale effects: Thermodynamic and hydrological aspects in a general circulation model." *Journal of Climate* 14(16): 3444–3463, https://doi.org/10.1175/1520-0442%282001%29014%3C3444%3AACPIMF%3E2.0.CO%3B2

Durkee, JD, and TL Mote. 2009. "A climatology of warm-season mesoscale convective complexes in subtropical South America." *International Journal of Climatology* 30(3): 418–431, https://doi.org/10.1002/joc.1893

Durkee, JD, TL Mote, and JM Shepherd. 2009. "The contribution of mesoscale convective complexes to rainfall across subtropical South America." *Journal of Climate* 22(17): 4590–4605, https://doi.org/10.1175/2009JCLI2858.1

Fan, J, B Han, A Varble, H Morrison, K North, P Kollias, B Chen, X Dong, SE Giangrande, A Khain, Y Lin, E Mansell, JA Milbrandt, R Stenz, G Thompson, and Y Wang. 2017. "Cloud-resolving model intercomparison of a MC3E squall line case: Part I – Convective updrafts." *Journal of Geophysical Research – Atmospheres* 122(17): 9351–9378, https://doi:10.1002/2017JD026622

Fridlind, AM, AS Ackerman, J-P Chaboureau, J Fan, WW Grabowski, AA Hill, TR Jones, MM Khaiyer, G Liu, P Minnis, H Morrison, L Nguyen, S Park, JC Petch, J-P Pinty, C Schumacher, BJ Shipway, AC Varble, X Wu, S Xie, and M Zhang. 2012. "A comparison of TWP-ICE observational data with cloud-resolving model results." *Journal of Geophysical Research – Atmospheres* 117(D5): D05204, https://doi.org/10.1029/2011JD016595

Fritsch, JM, RJ Kane, and CR Chelius. 1986. "The contribution of mesoscale convective weather systems to the warm-season precipitation in the United States." *Journal of Applied Meteorology and Climatology* 25(10): 1333–1345, https://doi.org/10.1175/1520-0450(1986)025<1333:TCOMCW>2.0.CO;2

Hagos, S, Z Feng, CD Burleyson, K-S S Lim, CN Long, D Wu, and G Thompson. 2014. "Evaluation of convection-permitting model simulations of cloud populations associated with the Madden-Julian Oscillation using data collected during the AMIE/DYNAMO field campaign." *Journal of Geophysical Research – Atmospheres* 119(21): 12,052–12,068, https://doi.org/10.1002/2014JD022143

Han, B., J. Fan, A. Varble, H. Morrison, CR Williams, B Chen, X Dong, SE Giangrande, A Khain, E Mansell, JA Milbrandt, J Shpund, and G Thompson. 2019. "Cloud-resolving model intercomparison of an MC3E squall line case: Part II – Stratiform precipitation properties." *Journal of Geophysical Research – Atmospheres* 124(2): 1090–1117, https://doi.org/10.1029/2018JD029596

Hartmann, DL, HH Hendon, and RA Houze Jr. 1984. "Some implications of the mesoscale circulations in tropical cloud clusters for large-scale dynamics and climate." *Journal of the Atmospheric Sciences* 41(1): 113–121, https://doi.org/10.1175/1520-0469(1984)041<0113:SIOTMC>2.0.CO;2

Hohenegger, C, and B Stevens. 2013. "Preconditioning deep convection with cumulus congestus." *Journal of the Atmospheric Sciences* 70(2): 448–464, https://doi.org/10.1175/JAS-D-12-089.1

Houze, RA, Jr. 1989. "Observed structure of mesoscale convective systems and implications for large-scale heating." *Quarterly Journal of the Royal Meteorological Society* 115(487): 425–461, https://doi.org/10.1002/qj.49711548702

Houze, RA, Jr. 2004. "Mesoscale convective systems." *Review of Geophysics* 42(4): RG4003, https://doi.org/10.1029/2004RG000150

Lang, SE, W-K Tao, X Zeng, and Y Li. 2011. "Reducing the biases in simulated radar reflectivities from a bulk microphysics scheme: Tropical convective systems." *Journal of the Atmospheric Sciences* 68(10): 2306–2320, https://doi.org/10.1175/JAS-D-10-05000.1

Luo, Y, Y Wang, H Wang, Y Zheng, and H Morrison. 2010. "Modeling convective-stratiform precipitation processes on a Mei-Yu front with the Weather Research and Forecasting model: Comparison with observations and sensitivity to cloud microphysics parameterizations." *Journal of Geophysical Research – Atmospheres* 115(D18): D18117, https://doi.org/10.1029/2010JD013873

Matsui, T, X Zeng, W-K Tao, H Masunaga, WS Olson, and S Lang. 2009. "Evaluation of long-term cloud-resolving model simulations using satellite radiance observations and multifrequency satellite simulators." *Journal of Atmospheric and Oceanic Technology* 26(7): 1261–1274, https://doi.org/10.1175/2008JTECHA1168.1

Nesbitt SW, R Cifelli, and SA Rutledge. 2006. "Storm morphology and rainfall characteristics of TRMM precipitation features." *Monthly Weather Review* 134(10): 2702–2721, https://doi.org/10.1175/MWR3200.1

Nicolini, M, and YG Skabar. 2011. "Diurnal cycle in convergence patterns in the boundary layer east of the Andes and convection." *Atmospheric Research* 100(4): 377–390, https://doi.org/10.1016/j.atmosres.2010.09.019

Ovchinnikov, M, T Ackerman, R Marchand, and M Khairoutdinov. 2006: "Evaluation of the multiscale modeling framework using data from the Atmospheric Radiation Measurement program." *Journal of Climate* 19(9): 1716–1729, https://doi.org/10.1175/JCLI3699.1

Rasmussen, KL, and RA Houze, Jr. 2011. "Orogenic convection in South America as seen by the TRMM satellite." *Monthly Weather Review* 139(8): 2399–2420, https://doi.org/10.1175/MWR-D-10-05006.1

Rasmussen, KL, MD Zuluaga, and RA Houze, Jr. 2014. "Severe convection and lightning in subtropical South America." *Geophysical Research Letters* 41(20): 7359–7366, https://doi.org/10.1002/2014GL061767

Rasmussen, KL, MM Chaplin, MD Zuluaga, and RA Houze, Jr. 2016. "Contribution of extreme convective storms to rainfall in South America." *Journal of Hydrometeorology* 17(1): 353–367, https://doi.org/10.1175/JHM-D-15-0067.1

Rasmussen, KL, and RA Houze, Jr. 2016. "Convective initiation near the Andes in subtropical South America." *Monthly Weather Review* 144(6): 2351–2374, https://doi.org/10.1175/MWR-D-15-0068.1

Romatschke, U, and RA Houze, Jr. 2010. "Extreme summer convection in South America." *Journal of Climate* 23(14): 3761–3791, https://doi.org/10.1175/2010JCLI3465.1

Ruscica, RC, AA Sörensson, and CG Menéndez. 2015. "Pathways between soil moisture and precipitation in southeastern South America." *Atmospheric Science Letters* 16(3): 267–272, https://doi.org/10.1002/asl2.552

Salio, P, M Nicolini, and EJ Zipser. 2007. "Mesoscale convective systems over southeastern South America and their relationship with the South American low-level jet." *Monthly Weather Review* 135(4): 1290–1309, https://doi.org/10.1175/MWR3305.1

Schumacher, C, RA Houze, Jr., and I Kraucunas, 2004. "The tropical dynamical response to latent heating estimates derived from the TRMM precipitation radar." *Journal of the Atmospheric Sciences* 61(12): 1341–1358, https://doi.org/10.1175/1520-0469(2004)061<1341:TTDRTL>2.0.CO;2

Solman, SA, E Sanchez, P Samuelsson, R.P. da Rocha, L Li, J Marengo, NL Pessacg, ARC Remedio, SC Chou, H Berbery, H Le Treut, M de Castro and D Jacob. 2013. "Evaluation of an ensemble regional climate model simulations over South America driven by the ERA-Interim reanalyses: model performance and uncertainties." *Climate Dynamics* 41(5-6): 1139–1157, https://doi.org/10.1007/s00382-013-1667-2

Song, H, W Lin, Y Lin, AB Wolf, R Neggers, LJ Donner, AD Del Genio, and Y Liu. 2013. "Evaluation of precipitation simulated by seven SCMs against the ARM observations at the SGP site." *Journal of Climate* 26(15): 5467–5492, https://doi.org/10.1175/JCLI-D-12-00263.1

Sörensson, AA, and CG Menéndez. 2011. "Summer soil-precipitation coupling in South America." *Tellus* 63(1): 56–68, https://doi.org/10.1111/j.1600-0870.2010.00468.x

Stanford, MW, A Varble, E Zipser, JW Strapp, D Leroy, A Schwarzenboeck, R Potts, and A Protat. 2017. "A ubiquitous ice size bias in simulations of tropical deep convection." *Atmospheric Chemistry and Physics* 17(15): 9599–9621, https://doi.org/10.5194/acp-17-9599-2017

Storelvmo, T. 2012. "Uncertainties in aerosol direct and indirect effects attributed to uncertainties in convective transport mechanisms." *Atmospheric Research* 118: 357–369, https://doi.org/10.1016/j.atmosres.2012.06.022

Varble, A, AM Fridlind, EJ Zipser, AS Ackerman, J-P Chaboureau, J Fan, A Hill, SA McFarlane, J-P Pinty, and B Shipway. 2011. "Evaluation of cloud-resolving model intercomparison simulations using TWP-ICE observations: Precipitation and cloud structure." *Journal of Geophysical Research – Atmospheres* 116(D12): D12206, https://doi.org/10.1029/2010JD015180

Varble, A, EJ Zipser, AM Fridlind, P Zhu, AS Ackerman, J-P Chaboureau, S Collis, J Fan, A Hill, and B Shipway. 2014a. "Evaluation of cloud-resolving and limited area model intercomparison simulations using TWP-ICE observations: 1. Deep convective updraft properties." *Journal of Geophysical Research – Atmospheres* 119(24): 13,891–13,918, https://doi.org/10.1002/2013JD021371

Varble, A, EJ Zipser, AM Fridlind, P Zhu, AS Ackerman, J-P Chaboureau, J Fan, A Hill, B Shipway, and CR Williams. 2014b. "Evaluation of cloud-resolving and limited area model intercomparison simulations using TWP-ICE observations: 2. Precipitation microphysics." *Journal of Geophysical Research – Atmospheres* 119(24): 13,919–13,945, https://doi.org/10.1002/2013JD021372

Velasco, I, and JM Fritsch. 1987. "Mesoscale convective complexes in the Americas." *Journal of Geophysical Research –Atmospheres* 92(D8): 9591–9613, https://doi.org/10.1029/JD092iD08p09591

Winker, DM, JL Tuckett, BJ Getzewich, Z Liu, MA Vaughan, and RR Rogers. 2013. "The global 3-D distribution of tropospheric aerosols as characterized by CALIOP." *Atmospheric Chemistry and Physics* 13(6): 3345–3361, https://doi.org/10.5194/acp-13-3345-2013

Zipser, EJ, DJ Cecil, C Liu, SW Nesbitt, and DP Yorty. 2006. "Where are the most intense thunderstorms on Earth?" *Bulletin of the American Meteorological Society* 87(8): 1057–1071, https://doi.org/10.1175/BAMS-87-8-1057

ARM

www.arm.gov

U.S. DEPARTMENT OF ENERGY

Office of Science